Activation cross sections of proton-induced reactions on praseodymium up to 30 MeV

Masayuki Aikawa [a,b,c,*], Yukina Hanada [c], He Huang [c], Hiromitsu Haba [d]

[a] *Faculty of Science, Hokkaido University, Sapporo 060-0810, Japan*

[b] *Global Center for Biomedical Science and Engineering, Faculty of Medicine, Hokkaido University, Sapporo 060-8648, Japan*

[c] *Graduate School of Biomedical Science and Engineering, Hokkaido University, Sapporo 060-8638, Japan*

[d] *Nishina Center for Accelerator-Based Science, RIKEN, Wako 351-0198, Japan*

Abstract

Activation cross sections of proton-induced reactions on ^{141}Pr were measured. Stacked foil activation technique and γ-ray spectrometry were adopted to derive the cross sections. The production cross sections of ^{141,140,139m}Nd, and ^{139}Ce were determined up to 30 MeV. The physical yield of ^{140}Nd was deduced using the measured cross sections of the ^{141}Pr(p,2n)^{140}Nd reaction. The physical yields of the proton- and deuteron-induced reactions on ^{141}Pr and ^{3}He-induced reaction on ^{nat}Ce for ^{140}Nd production were compared.

Keyword

Neodymium-140; Praseodymium-140; Praseodymium target; Proton irradiation; Cross section; Excitation function

1. Introduction

There are many radionuclides available in nuclear medicine. One of such radionuclides is ^{140}Nd ($T_{1/2}$ = 3.37 d), which is expected as a ^{140}Nd/^{140}Pr generator for Positron Emission Tomography (PET) [1,2] and an Auger electron emitter for endoradiotherapy [3,4]. The radionuclide ^{140}Nd can be produced via charged-particle-induced reactions, of which cross sections studied earlier are scarce and scattered (see [5–7] and references therein). Therefore, reliable cross sections of the reactions are required to estimate production yields of the radionuclide and co-produced impurities. The production yields enable us to determine the best reaction and most effective energy range for practical use.

We have previously studied the deuteron-induced reaction on the monoisotopic element ^{141}Pr to produce ^{140}Nd [5]. In this paper, we focused on the proton-induced reaction on ^{141}Pr. Three experimental studies of the reaction for ^{140}Nd production [6,8,9] were found in a literature survey in the EXFOR library [10] and related references. The experimental cross section data in the literature are largely scattered and more reliable data are required. Therefore, we performed an experiment to obtain cross sections of the ^{141}Pr(p,2n)^{140}Nd reaction up to 30 MeV. Production cross sections of other radionuclides were measured simultaneously to

* Corresponding author: Masayuki AIKAWA (aikawa@sci.hokudai.ac.jp), Faculty of Science, Hokkaido University, Sapporo 060-0810, Japan

estimate radioactive impurities. The production cross sections of ^{141,140,139m}Nd, and ^{139}Ce were determined up to 30 MeV. The physical yield of the ^{141}Pr(p,2n)^{140}Nd reaction was deduced from the measured cross sections. We discussed the appropriate reaction to produce ^{140}Nd based on the deduced physical yields.

2. Experimental

We conducted an experiment using a 30-MeV proton beam at the K70-MeV AVF cyclotron in RIKEN. We adopted stacked-foil activation technique and high-resolution γ-ray spectrometry to determine the excitation functions.

We prepared a target consisting of pure metallic thin foils of ^{141}Pr, ^{nat}Ti, and ^{27}Al. The ^{nat}Ti foils were used for the ^{nat}Ti(p,x)^{48}V monitor reaction to assess the beam parameters and the target thicknesses. The ^{27}Al foils were interleaved to catch recoiled products. Two ^{141}Pr (purity: 99%, thickness: 100 μm, size: 25 × 25 mm^2), one ^{nat}Ti (purity: 99.5%, thickness: 20 μm, size: 100 × 100 mm^2) and one ^{27}Al (purity: >99%, thickness: 10 μm, size: 100 × 100 mm^2) foils were purchased from Nilaco Corp., Japan. The ^{141}Pr foils sealed under argon to avoid oxidation were unpacked one day before a beam irradiation. The side lengths and weight of each foil were measured to obtain foil thicknesses. The measured thicknesses of two ^{141}Pr, ^{nat}Ti and ^{27}Al foils were 68.6 and 68.5 mg/cm^2, 9.1 mg/cm^2 and 2.2 mg/cm^2, respectively. The large foils were cut into small pieces of 8 × 8 mm^2 to fit a target holder. Eighteen sets of the Pr-Al-Ti-Ti-Al foils were stacked in the target holder served as a Faraday cup.

The target was irradiated with a proton beam collimated to 3 mm diameter. The irradiation lasted for 15 min. The average intensity measured using the Faraday cup without suppression voltage was 201 nA. The primary beam energy measured using the time-of-flight method [11] was 30.2 ±0.1 MeV. Energy degradation in the stacked target was calculated using stopping powers obtained from the SRIM code [12]. The calculation of the energy degradation was assessed by using the monitor reaction.

The γ-ray spectrometry was performed using a high-purity germanium detector (ORTEC GEM30P4-70) and a dedicated software (SEIKO EG&G Gamma Studio). The efficiency of the detector was calibrated with an ^{152}Eu standard source (Japan Radioisotope Association) and a multiple γ-ray emitting point source (Eckert & Ziegler Isotope Products). The latter consisted of ten radionuclides, ^{57,60}Co, ^{85}Sr, ^{88}Y, ^{109}Cd, ^{113}Sn, ^{137}Cs, ^{139}Ce, ^{203}Hg, and ^{241}Am. γ rays emitted from each irradiated foil without chemical separation were measured. Each ^{141}Pr foil was measured together with the next ^{27}Al foil that caught recoiled products. The ^{141}Pr foils were measured 3-9 times to assess decay curves of products. The cooling times were from 1.7 h to 31.9 d and the dead time was kept below 7.5%. The experimental parameters in detail were summarized in Table 1. Nuclear data required for cross section derivation were retrieved from the online databases, NuDat 2.8 [13], LiveChart [14], Lund/LBNL Nuclear Data Search [15] and QCalc [16]. The retrieved nuclear data were summarized in Table 2.

Cross sections of the ^{nat}Ti(p,x)^{48}V monitor reaction were derived to assess the beam parameters and the target thicknesses. The γ line at 983.5 keV (I_γ = 99.98%) emitted from each second ^{nat}Ti foil was measured. The loss of recoiled products in the second foils was assumed to be compensated from the first ^{nat}Ti foils.

The cross sections were determined using the measured spectra and compared with the IAEA recommended values [17,18]. The older recommended values [17] were selected for the following correction procedure because the shape was more similar to that of the derived excitation function. According to the comparison, the peak position and amplitude were found to be slightly shifted. First, to fit the peak position, the thicknesses of the ^{141}Pr foils, which dominantly affected the energy degradation, were corrected by +2% within the uncertainty (2%). Secondly, to fit the peak amplitude, the beam intensity was corrected by -7%. The measured thicknesses of ^{nat}Ti and ^{27}Al were adopted without any correction. The cross sections using the corrected parameters agree with the recommended values [17] as shown in Fig. 1. The adopted parameters for deduction of cross sections were summarized in Table 1.

Table 1. Experimental parameters.

Target	
Measured (corrected) thickness (mg/cm^2)	Pr: 68.6 (70.0), 68.5 (69.9)
	Ti: 9.1
	Al: 2.2
Stack composition	18 sets of Pr-Al-Ti-Ti-Al foils
Beam	
Measured (corrected) current (nA)	201 (187)
Primary energy (MeV)	30.2 ±0.1
Irradiation time (min)	15.0
Measurement	
Series: Cooling time (distance, dead time)	Ser. 1: 1.7-5.1 h (5-100 cm, 0.4-7.5%)
	Ser. 2: 5.3-10.1 h (5-100 cm, 0.2-4.9%)
	Ser. 3: 10.4-26.5 h (3-100 cm, 0.0-1.7%)
	Ser. 4: 1.7-1.9 d (3-50 cm, 0.0-2.4%)
	Ser. 5: 2.1-2.2 d (50 cm, 0.1-2.2%)
	Ser. 6: 2.7-2.8 d (50 cm, 0.0-2.0%)
	Ser. 7: 5.3-5.7 d (50 cm, 0.0-1.2%)
	Ser. 8: 14.2-14.3 d (30 cm, 0.3-0.6%)
	Ser. 9: 31.3-31.9 d (10 cm, 0.1-0.7%)

Table 1. Reaction and decay data retrieved from online databases [13–16].

Nuclide	Half-life	Decay mode (%)	E_γ (keV)	I_γ (%)	Contributing reaction	Q-value (MeV)
^{141}Nd	2.49 h	ε+β$^+$ (100)	511.0	5.18(8)	^{141}Pr(p,n)	-2.6
			1126.91	0.80(3)		
			1292.64	0.46(5)		

^{140}Nd	3.37 d	ε (100)	-	-	^{141}Pr(p,2n)	-10.6
^{139m}Nd	5.50 h	ε+β$^+$ (87.0)	113.87	40(5)	^{141}Pr(p,3n)	-21.2
		IT (13.0)	511.0	3.3(14)		
			708.1	26.3(13)		
			738.2	35.1(7)		
			827.8	10.3(6)		
			982.2	26.3(9)		
^{140}Pr	3.39 min	ε+β$^+$ (100)	**511.0**	102.0(6)	^{141}Pr(p,d)	-7.2
			1596.1	0.49(4)	^{140}Nd decay	
^{139}Ce	137.641 d	ε (100)	**165.8575**	80(8)	^{141}Pr(p,^{3}He)	-6.7
					^{139}Pr decay	
^{48}V	15.97 d	ε+β$^+$ (100)	511.0	99.8(8)	^{nat}Ti(p,x)	
			983.53	99.98(4)		
			1312.106	98.2(3)		

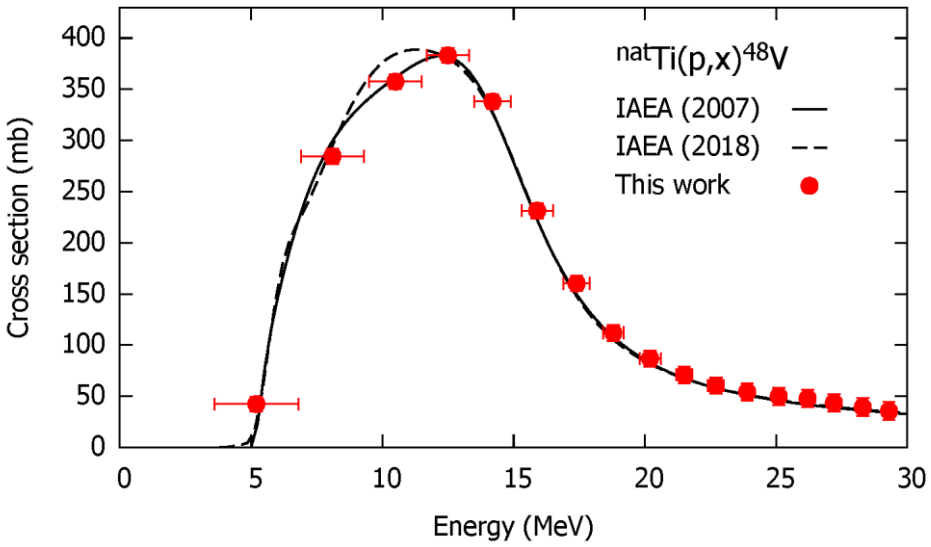

Fig. 1. Excitation function of the ^{nat}Ti(p,x)^{48}V monitor reaction with the recommended values [17,18].

3. Results and discussion

The production cross sections of ^{141,140,139m}Nd and ^{139}Ce were determined up to 30 MeV. The derived cross sections are summarized in Table 3. The results are graphically shown in Figs. 2-5 with the previous experimental data [6–9,19–22] and the theoretical model calculation in the TENDL-2019 library [23]. Physical yield of the ^{141}Pr(p,2n)^{140}Nd reaction was deduced using the measured cross sections as shown in Fig. 6.

The median projectile energy in each foil with the total uncertainty and the energy loss in paratheses is listed in Table 3. The total energy uncertainties of 0.1-2.2 MeV were propagated from the uncertainties of the primary beam energies (0.1 MeV) and foil thicknesses (1-2%). The total uncertainties of the cross sections of 8.9-21.9% were calculated from the square roots of the quadratic summation of the components; beam intensity (7%), γ-ray intensity (0.6-10.0%), detector efficiency (5%), target thickness (2%), target purity (1%) and counting statistics (0.5-17.4%).

Table 3. Production cross sections.

Energy (MeV)	^{141}Nd (mb)	^{140}Nd (mb)	^{139m}Nd (mb)	^{139}Ce (mb)
29.9 ±0.1 (0.3)		258 ±23	609 ±56	933 ±125
28.9 ±0.1 (0.3)		317 ±28	545 ±50	850 ±114
27.8 ±0.1 (0.3)		407 ±36	470 ±43	742 ±99
26.8 ±0.2 (0.3)		518 ±46	354 ±33	597 ±80
25.7 ±0.2 (0.3)		658 ±59	243 ±22	419 ±56
24.6 ±0.2 (0.4)		786 ±70	138 ±13	241 ±32
23.4 ±0.3 (0.4)	55.0 ±6.9	912 ±81	40.4 ±3.7	84.7 ±11.4
22.2 ±0.3 (0.4)	65.0 ±7.5	956 ±85	2.80 ±0.32	11.3 ±1.5
20.9 ±0.4 (0.4)	69.2 ±7.7	943 ±84		3.26 ±0.46
19.6 ±0.4 (0.4)	87.5 ±9.4	906 ±81		2.33 ±0.34
18.2 ±0.5 (0.4)	103 ±11	832 ±74		1.35 ±0.19
16.7 ±0.5 (0.5)	163 ±17	724 ±65		0.649 ±0.107
15.2 ±0.6 (0.5)	299 ±30	559 ±50		0.318 ±0.070
13.5 ±0.7 (0.6)	519 ±51	262 ±24		
11.6 ±0.9 (0.6)	577 ±56	34.8 ±3.3		
9.5 ±1.1 (0.7)	331 ±33	0.568 ±0.058		
7.0 ±1.4 (0.9)	59.5 ±6.0			
3.4 ±2.2 (1.4)	1.08 ±0.12			

3.1 The ^{141}Pr(p,n)^{141}Nd reaction

Cross sections of the ^{141}Pr(p,n)^{141}Nd reaction were measured. The isomer at 0.757 MeV of ^{141}Nd ($T_{1/2}$ = 62.0 s) that decays to the ground state (IT: 99.95%) and ^{141}Pr ($\varepsilon+\beta^+$: 0.05%) was produced simultaneously in the reaction. It completely decayed before the γ-ray spectrometry. We measured the γ line at 1126.91 keV (I_γ = 0.80%) with the decay of its ground state ($T_{1/2}$ = 2.49 h). The spectra measured after the cooling times of 1.7-5.1 h (Ser. 1) was used to derive the cross sections. The consistency of the cross sections was checked with those derived from another series (Ser. 2). The result is shown in Fig. 2 in comparison with the previous studies [6–8,20,21] and the theoretical model calculation in the TENDL-2019 library [23]. The experimental cross section data except those reported by Hogan (1971) were almost consistent with ours within the uncertainties. Only data of Hogan (1971) are largely different from the other experimental data. One possible reason for the discrepancy is the large difference in the amplitude of the ^{63}Cu(p,n)^{63}Zn monitor reaction. Their cross section of the monitor reaction at 15 MeV is 470 mb although the current IAEA recommended value is 322.3 mb normalized using the value of 222.9 mb in the ^{nat}Cu(p,n)^{63}Zn reaction [18] and the isotopic ratio of Cu (^{63}Cu: 69.15%, ^{65}Cu: 30.85%). The TENDL-2019 values agree well with ours.

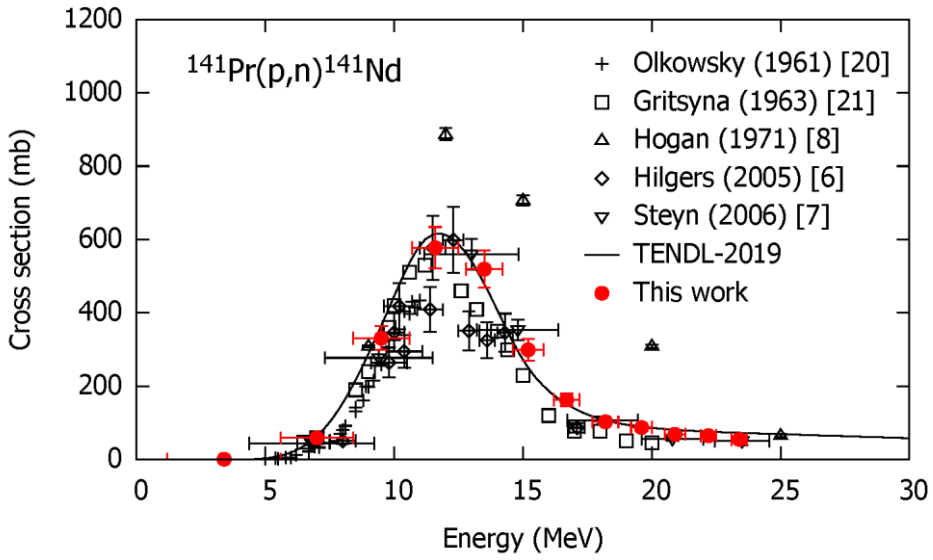

Fig. 2. Cross sections of the ^{141}Pr(p,n)^{141}Nd reaction with the previous data [6–8,20,21] and the TENDL-2019 values [23].

3.2 The ^{141}Pr(p,2n)^{140}Nd reaction

^{140}Nd has two metastable states, the ground state ($T_{1/2}$ = 3.37 d) and the isomer at 2.221 MeV ($T_{1/2}$ = 0.60 ms). The isomer fully decays to the ground state via the IT transition (IT: 100%). There are no measurable γ lines from ^{140}Nd. Thus the γ rays emitted with the decay of ^{140}Pr ($T_{1/2}$ = 3.39 min) were instead measured under the secular equilibrium with the decay of ^{140}Nd. Direct production of ^{140}Pr during irradiation was negligible due to cooling times much longer than its half-life. We measured the annihilation γ line at 511 keV (I_γ = 102%) emitted from the irradiated foils sandwiched with copper plates to force annihilation of the positrons (E_{mean} = 1067 keV). Decay curves of the 511-keV γ line using Ser. 5-7 were used to confirm negligible contribution of other positron emitters. Cross sections of the ^{141}Pr(p,2n)^{140}Nd reaction were derived using the spectra measured in Ser. 7. The result is compared with the previous studies [6,8,9] and the TENDL-2019 values [23] in Fig. 3. Our excitation function shows a smooth curve although previous studies by Hogan (1971) and by Hilgers et al. (2005) are largely scattered and different in amplitude at 20-28 MeV. The data of Zeisler et al. (1999) are different from ours in both amplitude and shape. The TENDL-2019 values slightly overestimate our experimental data below 23 MeV.

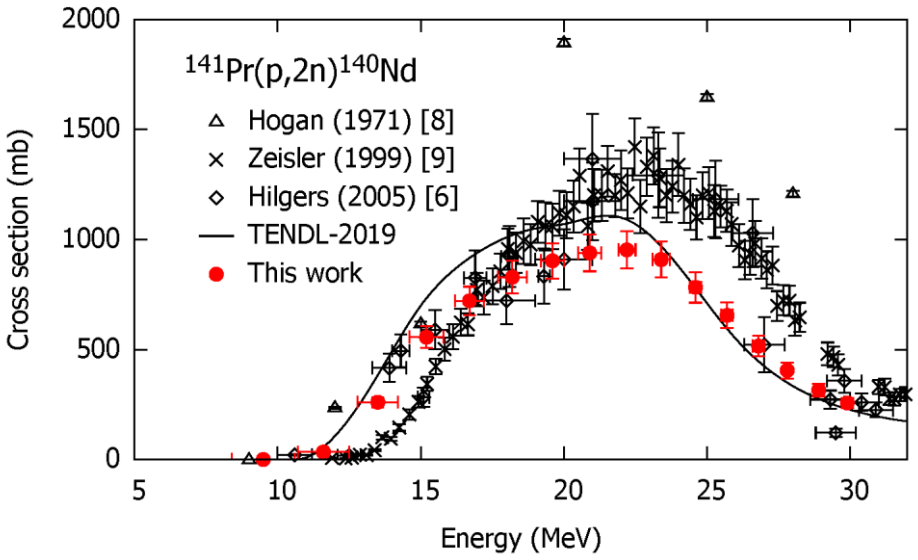

Fig. 3. Cross sections of the ^{141}Pr(p,2n)^{140}Nd reaction with the previous data [6,8,9] and the TENDL-2019 values [23].

3.3 The ^{141}Pr(p,3n)^{139m}Nd reaction

^{139m}Nd has a half-life of 5.50 h. We measured the γ line at 738.2 keV (I_γ = 35.1%) after the cooling times of 5.3-10.1 h (Ser. 2). The γ rays were emitted in the decay of ^{139m}Nd (IT: 11.80%, ε+β^+: 88.20%). The consistency was checked using another γ line at 113.87 keV in the same spectra and the same 738.2-keV γ line in another series (Ser. 3). The result shows a monotonic increase below 30 MeV as shown in Fig. 4. The excitation function is compared with the previous studies [7–9,22] and the TENDL-2019 values [23]. The data of Steyn et al. (2006) and Zeisler et al. (1999) are consistent with ours. The data of Hilgers et al. (2007) agree with ours below 28 MeV and deviate above 28 MeV. The data of Hogan (1971) are smaller than other experimental data. The TENDL-2019 values slightly overestimate the experimental data.

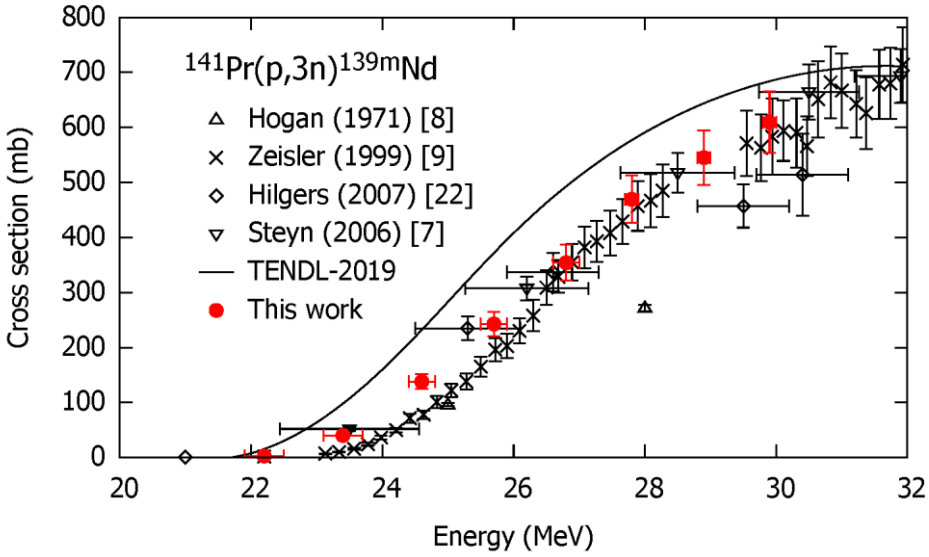

Fig. 4. Cross sections of the ^{141}Pr(p,3n)^{139m}Nd reaction with the previous data [7–9,22] and the TENDL-2019 values [23].

3.4 The ^{141}Pr(p,x)^{139}Ce reaction

To derive cross sections of the ^{141}Pr(p,x)^{139}Ce reaction, indirect production of ^{139}Ce ($T_{1/2}$ = 137.641 d) should be considered from the co-produced excited state and parent nuclei, ^{139m}Ce ($T_{1/2}$ = 54.8 s), ^{139}Pr ($T_{1/2}$ = 4.41 h), ^{139g}Nd ($T_{1/2}$ = 29.7 min), and ^{139m}Nd ($T_{1/2}$ = 5.50 h). The co-produced nuclei decayed completely during cooling times of about 31 d in Ser. 9. The measurement of the 165.8575-keV γ line (I_γ = 80%) emitted with the ^{139}Ce decay was performed. For the low energy γ line, the self-absorption effect was taken into account using the thicknesses of the ^{141}Pr foils and X-ray mass attenuation coefficients [24]. The measured net counts were corrected by +2.7% due to the self-absorption. The cumulative cross sections are shown in Fig. 5 in comparison with the previous data [6,19] and the TENDL-2019 values [23]. The data of both previous studies are in agreement with ours although some data points of Hilgers et al. (2005) are scattered. The TENDL-2019 values between 23 and 29 MeV are slightly larger than our result.

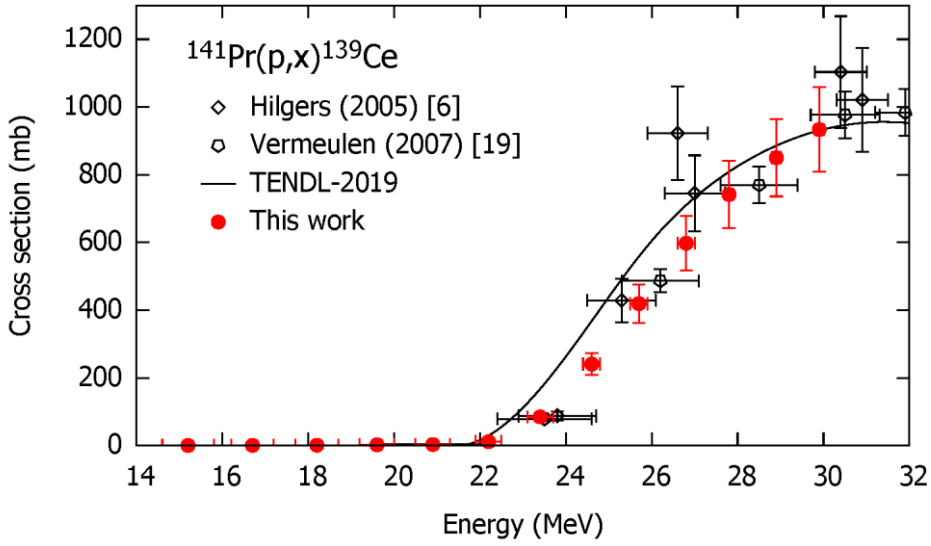

Fig. 5. Cross sections of the ^{141}Pr(p,x)^{139}Ce reaction with the previous data [6,19] and the TENDL-2019 values [23].

3.5 Physical yield

The physical yield for ^{140}Nd production was deduced from the measured cross sections of the ^{141}Pr(p,2n)^{140}Nd reaction. The result is compared with the experimental data [25] and the physical yields of the ^{141}Pr(d,3n)^{140}Nd [5] and ^{nat}Ce(^{3}He,x)^{140}Nd reactions [6] as shown in Fig. 6. The experimental data by Dmitriev and Molin [25] at 22 MeV agree with our deduced physical yield. The physical yield of the ^{141}Pr(p,2n)^{140}Nd reaction is larger than those of the ^{141}Pr(d,3n)^{140}Nd and ^{nat}Ce(^{3}He,x)^{140}Nd reactions. There are possible radioactive impurities of ^{141}Nd ($T_{1/2}$ = 2.49 h), ^{139g}Nd ($T_{1/2}$ = 29.7 min) and ^{139m}Nd ($T_{1/2}$ = 5.50 h). These impurities may be neglected for a ^{140}Nd/^{140}Pr generator because their half-lives are much shorter than ^{140}Nd ($T_{1/2}$ = 3.37 d). For application as an Auger electron emitter, the contribution of ^{139m}Nd should be eliminated. Therefore, the production of ^{140}Nd below the threshold energy of 22 MeV to produce ^{139m}Nd is considered. The physical yield of the ^{141}Pr(p,2n)^{140}Nd reaction reaches 29.6 GBq/C at 22 MeV. The physical yields of the ^{141}Pr(d,3n)^{140}Nd and ^{nat}Ce(^{3}He,x)^{140}Nd reactions reach only 7.14 and 0.240 GBq/C at 22 MeV. Based on the physical yields deduced from the experimental data, the proton-induced reaction on ^{141}Pr is preferred for ^{140}Nd production.

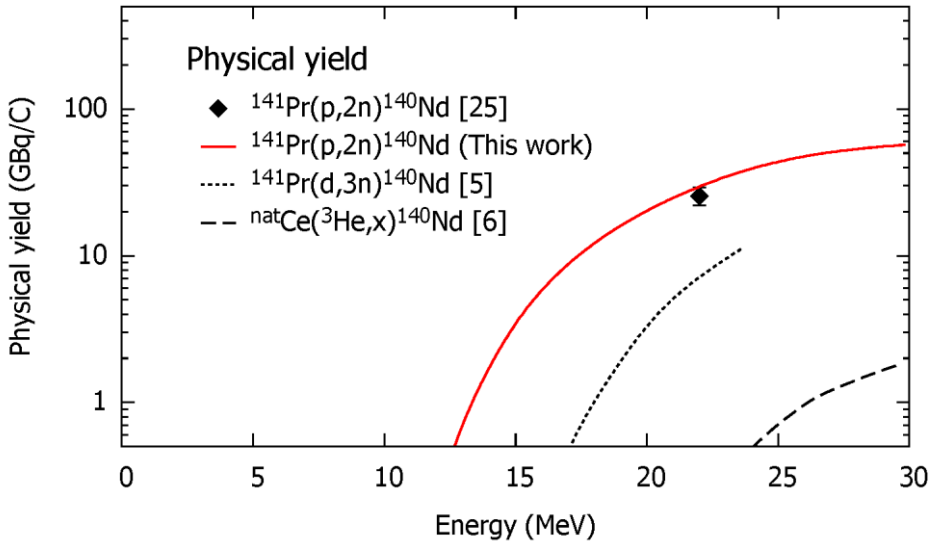

Fig. 6. Physical yield of the ^{141}Pr(p,2n)^{140}Nd reaction with the previous experimental data [25]. The physical yields deduced from the experimental cross sections of the ^{141}Pr(d,3n)^{140}Nd [5] and ^{nat}Ce(^{3}He,x)^{140}Nd reactions [6] are also shown for comparison.

4. Conclusion

We measured activation cross sections of the proton-induced reaction on ^{141}Pr. The experiment was performed at the RIKEN AVF cyclotron using the well-established methods, stacked-foil activation technique and high-resolution γ-ray spectrometry. The production cross sections of ^{141,140,139m}Nd and ^{139}Ce were determined. The derived cross sections are compared with the previous studies and the theoretical model calculation in the TENDL-2019 library. Physical yield of the ^{141}Pr(p,2n)^{140}Nd reaction was deduced and compared with those of the ^{141}Pr(d,3n)^{140}Nd and ^{nat}Ce(^{3}He,x)^{140}Nd reactions. Based on the comparison, we conclude that the ^{141}Pr(p,2n)^{140}Nd reaction is preferable for ^{140}Nd production. The experimental result is expected to contribute to the research and development of nuclear medicine using a ^{140}Nd/^{140}Pr generator and Auger electron emitter.

Acknowledgment

This work was carried out at RI Beam Factory operated by RIKEN Nishina Center and CNS, University of Tokyo, Japan.

Declarations of interest

None.

Reference

[1] K.P. Zhernosekov, D. V. Filosofov, S.M. Qaim, F. Rosch, A ^{140}Nd/^{140}Pr radionuclide generator based on physico-chemical transitions in ^{140}Pr complexes after electron capture decay of ^{140}Nd-DOTA, Radiochim. Acta. 95 (2007) 319–327. https://doi.org/10.1524/ract.2007.95.6.319.

[2] S.K. Zeisler, D.W. Becker, A New Method for PET Imaging of Tumors Human Serum Albumin Labeled with the Long-lived Nd-140/Pr-140 In Vivo Radionuclide Generator, Clin. Positron Imaging. 2 (1999) 324. https://doi.org/10.1016/S1095-0397(99)00084-9.

[3] F. Rösch, J. Brockmann, N.A. Lebedev, S.M. Qaim, The auger-electron emitter ^{140}Nd: production and radiochemical separation, J. Label. Compd. Radiopharm. Suppl. 1 (1999) S927–S929.

[4] F. Rösch, J. Brockmann, N.A. Lebedev, S.M. Qaim, Production and Radiochemical Separation of the Auger Electron Emitter 140Nd, Acta Oncol. (Madr). 39 (2000) 727–730. https://doi.org/10.1080/028418600750063794.

[5] M. Aikawa, T. Maehashi, D. Ichinkhorloo, S. Ebata, Y. Komori, H. Haba, Activation cross sections of deuteron-induced reactions on praseodymium up to 24 MeV, Nucl. Instruments Methods Phys. Res. Sect. B Beam Interact. with Mater. Atoms. 498 (2021) 23–26. https://doi.org/10.1016/j.nimb.2021.04.011.

[6] K. Hilgers, Y.N. Shubin, H.H. Coenen, S.M. Qaim, Experimental measurements and nuclear model calculations on the excitation functions of ^{nat}Ce(^{3}He, xn) and ^{141}Pr(p,xn) reactions with special reference to production of the therapeutic radionuclide ^{140}Nd, Radiochim. Acta. 93 (2005) 553–560.

https://doi.org/10.1524/ract.2005.93.9-10.553.

[7] G.F. Steyn, C. Vermeulen, F.M. Nortier, F. Szelecsényi, Z. Kovács, S.M. Qaim, Production of no-carrier-added ^{139}Pr via precursor decay in the proton bombardment of ^{nat}Pr, Nucl. Instruments Methods Phys. Res. Sect. B Beam Interact. with Mater. Atoms. 252 (2006) 149–159. https://doi.org/10.1016/j.nimb.2006.08.012.

[8] J.J. Hogan, Study of the ^{141}Pr(p,xn) reaction from 10-85 MeV, J. Inorg. Nucl. Chem. 33 (1971) 3627–3641. https://doi.org/10.1016/0022-1902(71)80267-1.

[9] S.K. Zeisler, D.W. Becker, Production of the ^{140}Nd/^{140}Pr radionuclide generator for biomedical studies, J. Label. Compd. Radiopharm. Suppl. 1 (1999) S921–S923.

[10] N. Otuka, E. Dupont, V. Semkova, B. Pritychenko, A.I. Blokhin, M. Aikawa, S. Babykina, M. Bossant, G. Chen, S. Dunaeva, R.A. Forrest, T. Fukahori, N. Furutachi, S. Ganesan, Z. Ge, O.O. Gritzay, M. Herman, S. Hlavač, K. Kato, B. Lalremruata, Y.O. Lee, A. Makinaga, K. Matsumoto, M. Mikhaylyukova, G. Pikulina, V.G. Pronyaev, A. Saxena, O. Schwerer, S.P. Simakov, N. Soppera, R. Suzuki, S. Takács, X. Tao, S. Taova, F. Tárkányi, V. V. Varlamov, J. Wang, S.C. Yang, V. Zerkin, Y. Zhuang, Towards a More complete and accurate experimental nuclear reaction data library (EXFOR): International collaboration between nuclear reaction data centres (NRDC), Nucl. Data Sheets. 120 (2014) 272–276. https://doi.org/10.1016/j.nds.2014.07.065.

[11] T. Watanabe, M. Fujimaki, N. Fukunishi, H. Imao, O. Kamigaito, M. Kase, M. Komiyama, N. Sakamoto, K. Suda, M. Wakasugi, K. Yamada, Beam energy and longitudinal beam profile measurement system at the RIBF, in: Proc. 5th Int. Part. Accel. Conf. (IPAC 2014), 2014: pp. 3566–3568.

[12] J.F. Ziegler, J.P. Biersack, M.D. Ziegler, SRIM: the Stopping and Range of Ions in Matter, (2008). http://www.srim.org.

[13] National Nuclear Data Center, Nuclear structure and decay data on-line library, Nudat 2.8, (2019). http://www.nndc.bnl.gov/nudat2/.

[14] International Atomic Energy Agency, LiveChart of Nuclides, (2009). https://www-nds.iaea.org/livechart/.

[15] S.Y.F. Chu, L.P. Ekström, R.B. Firestone, The Lund/LBNL Nuclear Data Search, (1999). http://nucleardata.nuclear.lu.se/toi/.

[16] B. Pritychenko, A. Sonzogni, Q-value Calculator (QCalc), (2003). http://www.nndc.bnl.gov/qcalc/.

[17] F. Tárkányi, S. Takács, K. Gul, A. Hermanne, M.G. Mustafa, M. Nortier, P. Obložinský, S.M. Qaim, B. Scholten, Y.N. Shubin, Z. Yousiang, Monitor Reactions 2007, updated version of charged particle cross-section database for medical radioisotope production, IAEA-TECDOC-1211, (2007). https://www-nds.iaea.org/medical/medical-old/monitor_reactions.html.

[18] A. Hermanne, A. V. Ignatyuk, R. Capote, B. V. Carlson, J.W. Engle, M.A. Kellett, T. Kibédi, G. Kim, F.G. Kondev, M. Hussain, O. Lebeda, A. Luca, Y. Nagai, H. Naik, A.L. Nichols, F.M. Nortier, S. V. Suryanarayana, S. Takács, F.T. Tárkányi, M. Verpelli, Reference Cross Sections for Charged-particle

Monitor Reactions, Nucl. Data Sheets. 148 (2018) 338–382. https://doi.org/10.1016/j.nds.2018.02.009.

[19] C. Vermeulen, G.F. Steyn, F.M. Nortier, F. Szelecsényi, Z. Kovács, S.M. Qaim, Production of ^{139}Ce by proton-induced reactions on ^{141}Pr and ^{nat}La, Nucl. Instruments Methods Phys. Res. Sect. B Beam Interact. with Mater. Atoms. 255 (2007) 331–337. https://doi.org/10.1016/j.nimb.2006.12.145.

[20] J. Olkowsky, M. Le Pape, I. Gratot, Fonction d'excitation de ^{141}Pr(p,n)^{141}Nd Jusqu'à 11.1 MeV, Nucl. Phys. 23 (1961) 164–168. https://doi.org/10.1016/0029-5582(61)90250-4.

[21] V.T. Gritsyna, A.P. Klyucharev, V. V. Remaev, L.N. Reshetova, Ratio of the cross sections for the production of the isomer and ground states of nuclei in the (p,n) reaction at energies from the threshold to 20 MeV, Sov. Phys. JETP. 17 (1963) 1186–1189.

[22] K. Hilgers, S. Sudár, S.M. Qaim, Formation of the isomeric pairs 139Ndm,g and 141Ndm,g in proton and 3He-particle-induced nuclear reactions, Phys. Rev. C. 76 (2007). https://doi.org/10.1103/PhysRevC.76.064601.

[23] A.J. Koning, D. Rochman, J. Sublet, N. Dzysiuk, M. Fleming, S. van der Marck, TENDL: Complete Nuclear Data Library for Innovative Nuclear Science and Technology, Nucl. Data Sheets. 155 (2019) 1–55. https://doi.org/10.1016/j.nds.2019.01.002.

[24] J.H. Hubbel, S.M. Seltzer, X-Ray Mass Extinction Coefficients, NIST Stand. Ref. Database 126. (2004). https://doi.org/https://doi.org/10.18434/T4D01F.

[25] P.P. Dmitriev, G.A. Molin, Radionuclide Yields for Thick Targets at 22 MeV Proton Energy, INDC(CCP)-188/L, 1982.